

TRB3 Gene Silencing Alleviates Diabetic Cardiomyopathy in a Type 2 Diabetic Rat Model

Yun Ti, Guo-lu Xie, Zhi-hao Wang, Xiao-lei Bi, Wen-yuan Ding, Jia Wang, Gui-hua Jiang, Pei-li Bu, Yun Zhang, Ming Zhong, and Wei Zhang

OBJECTIVE—Tribbles 3 (TRB3) is associated with insulin resistance, an important trigger in the development of diabetic cardiomyopathy (DCM). We sought to determine whether TRB3 plays a major role in modulating DCM and the mechanisms involved.

RESEARCH DESIGN AND METHODS—The type 2 diabetic rat model was induced by high-fat diet and low-dose streptozotocin. We evaluated the characteristics of type 2 DCM by serial echocardiography and metabolite tests, Western blot analysis for TRB3 expression, and histopathologic analyses of cardiomyocyte density, lipids accumulation, cardiac inflammation, and fibrosis area. We then used gene silencing to investigate the role of TRB3 in the pathophysiologic features of DCM.

RESULTS—Rats with DCM showed severe insulin resistance, left ventricular dysfunction, aberrant lipids deposition, cardiac inflammation, fibrosis, and TRB3 overexpression. We found that the silencing of *TRB3* ameliorated metabolic disturbance and insulin resistance; myocardial hypertrophy, lipids accumulation, inflammation, fibrosis, and elevated collagen I-to-III content ratio in DCM rats were significantly decreased. These anatomic findings were accompanied by significant improvements in cardiac function. Furthermore, with *TRB3* gene silencing, the inhibited phosphorylation of Akt was restored and the increased phosphorylation of extracellular signal-regulated kinase 1/2 and Jun NH₂-terminal kinase in DCM was significantly decreased.

CONCLUSIONS—*TRB3* gene silencing may exert a protective effect on DCM by improving selective insulin resistance, implicating its potential role for treatment of human DCM. *Diabetes* 60:2963–2974, 2011

Diabetic cardiomyopathy (DCM), which occurs in patients with diabetes, carries a substantial risk concerning the subsequent development of heart failure and increased mortality (1). Different pathophysiological stimuli are involved in its development and mediate tissue injury leading to left ventricle (LV) systolic and diastolic dysfunction. Insulin resistance is considered to play a causal role in the pathogenesis and development of DCM (2–4). Insulin resistance is associated with increased LV mass (5) and deterioration of LV diastolic

function (6). However, the underlying relevance of insulin resistance leading to altered myocardial structure remains incompletely understood.

Tribbles 3 (TRB3) is a pseudokinase with increased activity in response to fasting that binds to and inhibits the activation of the serine-threonine kinase Akt in the liver (7,8). Indeed, humans with a gain-of-function mutation in TRB3 show increased insulin resistance and diabetes-associated complications (9,10). These observations have led to the suggestion that TRB3 elevation contributes to insulin resistance. TRB3 also serves as a molecular switch and regulates the activation of the three classes of mitogen-activated protein kinases (MAPKs) (11). TRB3 binds to and regulates MAPK kinase, thus controlling the activation of MAPK by incoming signals (11). However, the TRB3/MAPK signal-transduction pathway has not been investigated in vivo on cardiac tissues directly.

Akt and MAPK are the most important pathways involved in selective insulin resistance (12), and activated MAPK contributes to the development of cardiac fibrosis (13–15). Thus, we hypothesized that upregulated TRB3 induced by insulin resistance might participate in the pathophysiological process of DCM. First, we established the type 2 DCM model and determined the relationships among TRB3 expression, cardiac remodeling, and cardiac function in the model. To further elucidate the role of TRB3 in DCM, we used *TRB3* gene silencing in vivo to explore the mechanisms of TRB3 in DCM as a potential target for treatment.

RESEARCH DESIGN AND METHODS

Induction of diabetes. Sixty male Sprague-Dawley rats (120–140 g) were purchased from the experimental animal center of Shandong University of Traditional Chinese Medicine (Ji'nan, China). The animals were housed at 22°C with 12-h light-dark cycles. After 1 week of acclimatization, intraperitoneal glucose tolerance test (IPGTT) and intraperitoneal insulin tolerance test (IPITT) were performed. The rats were then randomized into four groups: control, chow + streptozotocin (STZ), high-fat (HF) diet, and diabetes. HF and diabetic groups were fed an HF diet (34.5% fat, 17.5% protein, 48% carbohydrate; Beijing HFK Bio-Technology, China), and the other two groups received normal chow. Four weeks later, IPGTT and IPITT were performed again, and blood was sampled through the jugular vein. Fasting blood glucose (FBG) and fasting insulin were measured, and the insulin sensitivity index [ISI = ln(FBG × fasting insulin)⁻¹] was calculated. Diabetes was induced by a single intraperitoneal injection of STZ (Sigma, St. Louis, MO; 27.5 mg/kg i.p. in 0.1 mol/L citrate buffer, pH 4.5) to rats with insulin resistance. Rats in the chow + STZ group received the same dose of STZ. The control and HF groups received citrate buffer (intraperitoneally) alone. One week after STZ administration, rats with FBG >11.1 mmol/L in two consecutive analyses were considered the diabetic rat model. After 16 weeks of diabetes, rats were killed. All experimental procedures were performed in accordance with animal protocols approved by the Shandong University Animal Care Committee.

IPGTT and IPITT. Glucose tolerance was assessed by IPGTT after rats fasted for 12 h. A bolus of glucose (1 g/kg i.p.) was injected, and blood samples were collected sequentially from the tail vein at 0, 15, 30, 60, and 120 min and tested for glucose. Plasma glucose was measured with a One-Touch Glucometer (LifeScan, Milpitas, CA). The mean area under the receiver operating characteristic curve (AUC) was calculated for glucose.

From the Key Laboratory of Cardiovascular Remodeling and Function Research, Qilu Hospital of Shandong University, Chinese Ministry of Education and Chinese Ministry of Health, Ji'nan, Shandong Province, China, and the Department of Cardiology, Qilu Hospital of Shandong University, Ji'nan, Shandong Province, China.

Corresponding author: Wei Zhang, zhangweisdu@gmail.com, or Ming Zhong, zhongmingzm@gmail.com.

Received 25 April 2011 and accepted 18 August 2011.
DOI: 10.2337/db11-0549

This article contains Supplementary Data online at <http://diabetes.diabetesjournals.org/lookup/suppl/doi:10.2337/db11-0549/-/DC1>.

Y.T. and G.-L.X. contributed equally to this study.

© 2011 by the American Diabetes Association. Readers may use this article as long as the work is properly cited, the use is educational and not for profit, and the work is not altered. See <http://creativecommons.org/licenses/by-nc-nd/3.0/> for details.

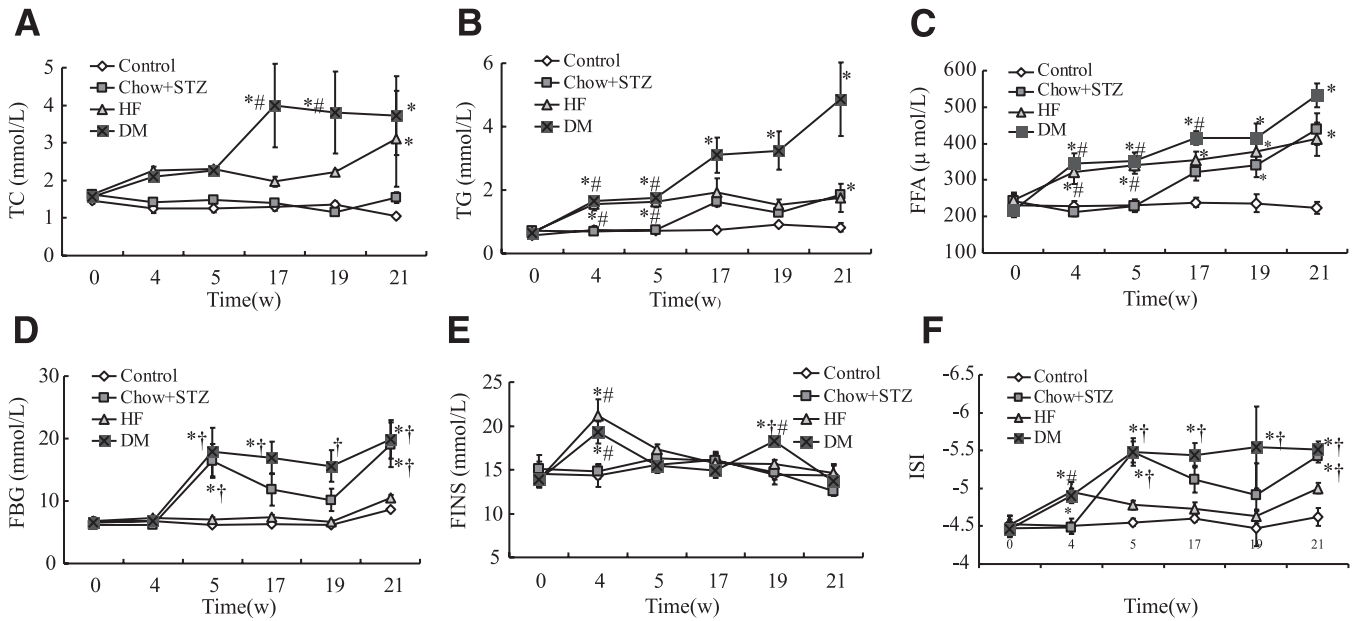


FIG. 1. Diabetic (DM) rats show metabolic disturbance. A: Total cholesterol (TC) levels. B: Triglyceride (TG) levels. C: FFAs. D: FBG. E: Fasting insulin (FINS). F: ISI. Data are mean ± SEM; n = 7–10 per group. *P < 0.05 vs. control; †P < 0.05 vs. HF; #P < 0.05 vs. chow + STZ. w, weeks.

To evaluate insulin tolerance, IPITT was performed after rats fasted for 4 h. A bolus of insulin (1 unit/kg i.p.) was administered, and blood samples were taken for glucose measurement as described above.

Blood analyses. After rats fasted overnight, we collected jugular blood. Total cholesterol, triglyceride levels, and FBG were analyzed with use of the Bayer 1650 blood chemistry analyzer (Bayer, Tarrytown, NY). Free fatty acid (FFA) concentrations were measured using an enzymatic test kit (CSB-E08770r; HuaMei BIO-TECH, Wuhan, China). Fasting insulin level was measured by enzyme-linked immunosorbent assay. ISI was calculated.

Echocardiography and measurement of blood pressure. Echocardiography involved use of the Vevo770 imaging system (VisualSonics, Toronto, Canada). Images were obtained from two-dimensional, M-mode, pulsed-wave Doppler and tissue Doppler imaging. All measurements were performed by the same observer and were the average of six consecutive cardiac cycles. Wall thickness and LV dimensions were obtained from a long-axis view at the level of chordae tendineae. Diameters of left ventricular end diastole, left ventricular end-diastolic posterior wall, and septum thickness, as well as left ventricular ejection fraction (LVEF) and fractional shortening (FS), were measured according to the American Society of Echocardiography guidelines (16). The mitral-valve pulsed Doppler recordings were obtained from the apical four-chamber view. After pulsed Doppler, we evaluated transmitral flow velocity variables, including peak E, peak A, and the E-to-A (E/A) ratio. Isovolumetric contraction time, isovolumetric relaxation time, and ejection time were measured and were used to calculate the Tei index (Tei index = Isovolumetric contraction time + isovolumetric relaxation time/ejection time). The tissue Doppler imaging of the mitral annulus was obtained from the apical four-chamber view. We analyzed early (E') and late (A') diastolic velocity and calculated E'/A' and E/E'.

For quantitative analysis of integrated backscatter (IBS) of the LV, we used a commercially available software package (acoustic densitometry; Phillips Medical Systems, Netherlands) (17). Two-dimensional echocardiographic images, including LV long-axis and apical four-chamber views, were obtained. The following variables were measured: time-averaged IBS, cyclic variation of integrated backscatter (CVIB), and standardized IBS (IB%).

Heart rate, systolic blood pressure, diastolic blood pressure, and mean arterial pressure were measured with a noninvasive tail-cuff system (Softron BP-98A; Softron, Tokyo, Japan) as described previously (18).

Hemodynamic measurement. Rats under deep anesthesia underwent hemodynamic measurement. A fluid-filled catheter was advanced from the right carotid artery into the LV, and the left ventricular end diastolic pressure (LVEDP) was measured.

Histology and morphometric analysis. Paraformaldehyde (4%) fixed hearts were bisected transversely at the midventricular level, embedded in paraffin, and cut into 4-µm sections. A single myocyte was measured with images captured from hematoxylin and eosin-stained sections. The myocyte cross-sectional area was assessed under ×400 magnification within the LV, and

a mean was obtained by quantitative morphometry with automated image analysis (Image-Pro Plus, Version 5.0; Media Cybernetics, Houston, TX).

Dark green-stained collagen fibers were quantified as a measure of fibrosis in Masson trichrome-stained sections. The collagen volume fraction (CVF) and perivascular collagen area/luminal area (PVCA/LA) were analyzed by quantitative morphometry with automated image analysis (Image-Pro Plus, Version 5.0). CVF was calculated as reported previously (19). Perivascular collagen was excluded from the CVF measurement. To normalize the PVCA around vessels with different sizes, the perivascular collagen content was represented as the PVCA-to-LA ratio.

Interstitial and perivascular fibrosis were evaluated by Picrosirius red staining. Sections were stained with 0.5% sirius red (Sigma) in saturated picric acid for 25 min. Collagen was stained red.

Myocardial frozen sections (5 µm) were stained with Oil Red O (Sigma) for 10 min, washed, and then counterstained with hematoxylin for 30 s. A Nikon microscope (Nikon, Melville, NY) was used to capture the Oil Red O-stained tissue sections.

Hydroxyproline analysis. The collagen content of myocardial tissue was determined by hydroxyproline assay (20). Tissue hydrolysate was detected by use of an ELISA kit (F15649; Westang Bio-Tech, Shanghai, China). Data were expressed as micrograms collagen per milligram dry weight, with the assumption that collagen contains an average of 13.5% hydroxyproline (21).

Immunohistochemical staining. Paraffin sections underwent immunohistochemistry by a microwave-based antigen retrieval method. The sections were incubated with primary rabbit polyclonal anti-collagen I, anti-collagen III, anti-tumor necrosis factor (TNF)-α, and anti-interleukin (IL)-6 antibodies (Abcam, Cambridge, MA) overnight and then with a matching biotinylated secondary antibody for 30 min at 37°C. Negative controls were omission of the primary antibody. The stained sections were developed with diaminobenzidine and counterstained with hematoxylin. The results were viewed under a confocal FV 1000 SPD laser scanning microscope (Olympus, Japan).

Quantitative real-time RT-PCR. Total RNA was prepared with the TRIzol reagent (Gibco/Invitrogen, Carlsbad, CA). RT-PCR was performed using the following primers: β-actin, forward 5'-AGA CCT TCA ACA CCC CAG-3' and reverse 5'-CAC GAT TTC CCT CTC AGC-3'; brain natriuretic protein, forward 5'-GGG CTG TGA CGG GCT GAG GTT-3' and reverse 5'-AGT TTG TGC TGG AAG ATA AGA3'-; TRB3, forward 5'-TGA TGC TGT CTG GAT GAC AA-3' and reverse 5'-GTG AAT GGG GAC TTT GGT CT-3'; TNF-α, forward 5'-CAC GCT CTT CTG TCT ACT GA-3' and reverse 5'-GGA CTC CGT GAT GTC TAA GT-3'; and IL-6, forward 5'-ACC ACT TCA CAA GTC GGA GG-3' and reverse 5'-ACA GTG CAT CAT CGC TGT TC-3'. Reactions were carried out on a real-time PCR thermocycler (IQ5 Real-Time PCR cyler; Bio-Rad), using SYBR green as fluorescence dye. Relative expression analysis involved the 2^{-ΔΔCT} method.

Western blot analysis. Western blot analysis was as described previously (22). We used antibodies against TRB3 (Calbiochem, La Jolla, CA), collagen I, collagen III, TNF-α, IL-6 (Abcam), phospho (p)-extracellular signal-regulated

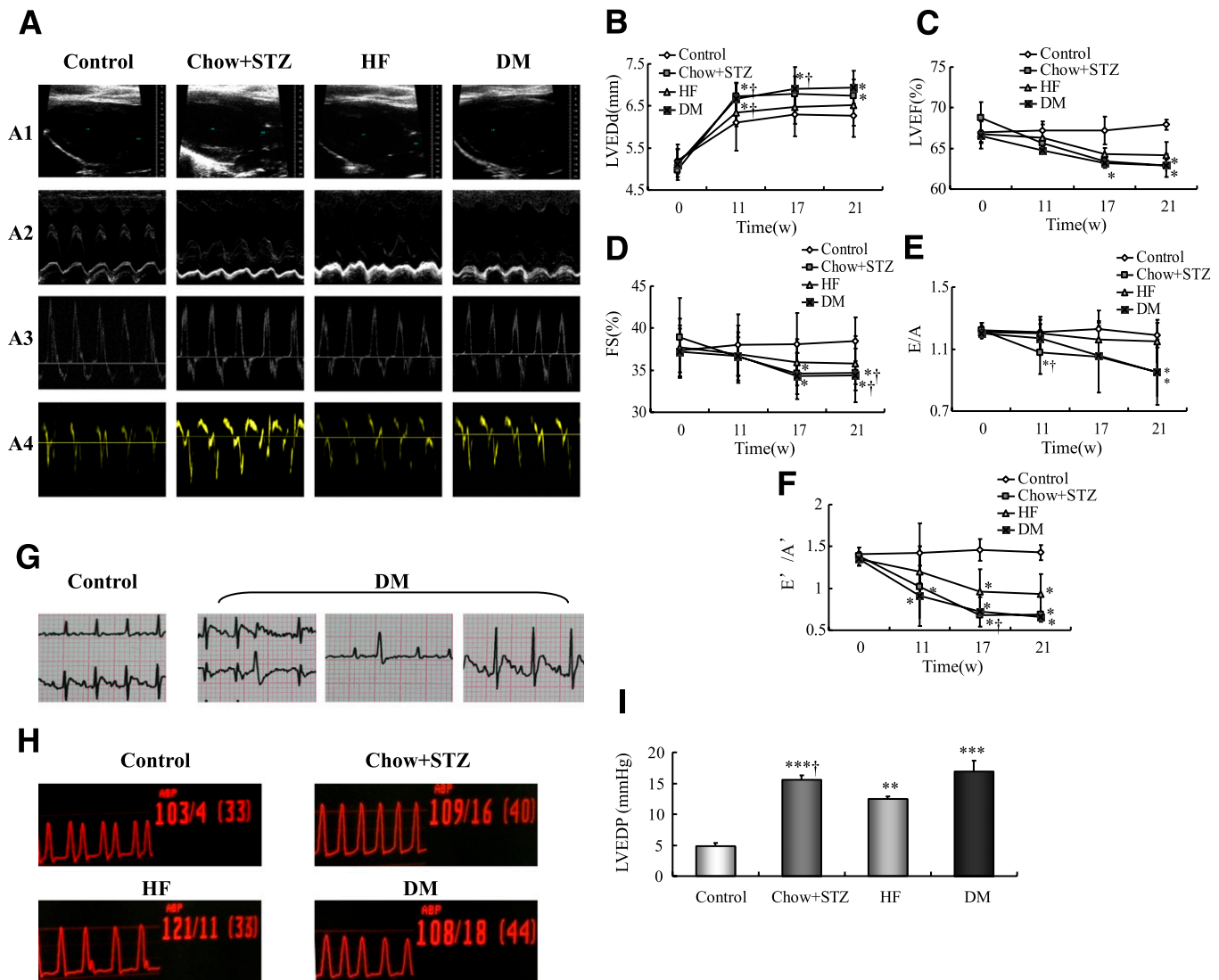


FIG. 2. Deterioration of cardiac function in diabetic (DM) rats. **A1:** Representative two-dimensional echocardiograms. **A2:** Representative M-mode echocardiograms. **A3:** Representative pulsed-wave Doppler echocardiograms of mitral inflow. **A4:** Representative tissue Doppler echocardiograms. **B–F:** Sequential evaluations of left ventricular end diastolic diameter (LVEDd) (**B**), LVEF (**C**), FS (**D**), E/A (**E**), and E'/A' (**F**). **G:** Electrocardiogram of control and DM groups at the end of the experiment. **H:** Pressure curves of cardiac catheterization. **I:** Analysis of LVEDP. Data are mean \pm SEM; $n = 7$ –10 per group. * $P < 0.05$, ** $P < 0.01$, *** $P < 0.001$ vs. control; † $P < 0.05$ vs. HF. w, weeks. (A high-quality digital representation of this figure is available in the online issue.)

kinase (ERK)/ERK, p-p38/p38 MAPK, p-Jun NH₂-terminal kinase (JNK)/JNK, and p-Akt/Akt (Cell Signaling Technology, Beverly, MA), followed by anti-IgG horseradish peroxidase-conjugated secondary antibody. TRB3, collagen I, collagen III, TNF- α , and IL-6 protein levels were normalized to that of β -actin as an internal control and phosphospecific proteins to that of total protein.

Gene silencing of TRB3. Sixty rats were randomized to receive TRB3 small interfering RNA (siRNA) or vehicle treatment. Gene silencing occurred immediately after the appearance of LV diastolic dysfunction. After 12 weeks of diabetes, both E/A and E'/A' were < 1.0 as assessed by echocardiography in diabetic rats. Animals were then injected via the jugular vein with 2.5×10^{10} plaque-forming units of an adenovirus harboring TRB3 gene (TRB3-siRNA) or a control empty virus (vehicle). Adenovirus transfer was repeated in 2 weeks. According to our present and previous studies (23), TRB3 level was increased in HF diet-fed and high fructose-fed rats. Previous studies have shown that insulin resistance was a hallmark of obesity (24) and metabolic syndrome (25). In light of the interaction between TRB3 and insulin resistance, we also investigated the effect of TRB3-siRNA on HF diet-induced cardiac injury. Four weeks after the first adenovirus injection, rats were killed. The heart was excised and weighed. **Statistical analysis.** Values are presented as mean \pm SEM. SPSS 16.0 (SPSS, Chicago, IL) was used for statistical analysis. Results were compared by one-way ANOVA, followed by Tukey-Kramer post hoc test and independent samples t test. A $P < 0.05$ was considered statistically significant.

RESULTS

Generation of type 2 DCM model

General characteristics of diabetic rats. As expected, the rats in the diabetic group had the highest values of water intake, food intake, and urine volume compared with the other three groups ($P < 0.01 \sim P < 0.001$). Heart weight was significantly higher in the diabetic group than in the control and chow + STZ groups ($P < 0.01$) (Supplementary Table 1).

Glucose and insulin tolerance. After a 4-week HF diet, insulin resistance was confirmed by IPGTT and IPITT. By IPGTT, the levels of blood glucose in the diabetic group were significantly higher at week 4 than at baseline at all of the time points tested except at 15 min (Supplementary Fig. 1A1). The AUC across the time for glucose level was higher at week 4 than at baseline (29.08 ± 1.27 vs. 25.09 ± 0.73 , respectively; $P < 0.05$) (Supplementary Fig. 1A2). Similarly, IPITT revealed impaired insulin sensitivity

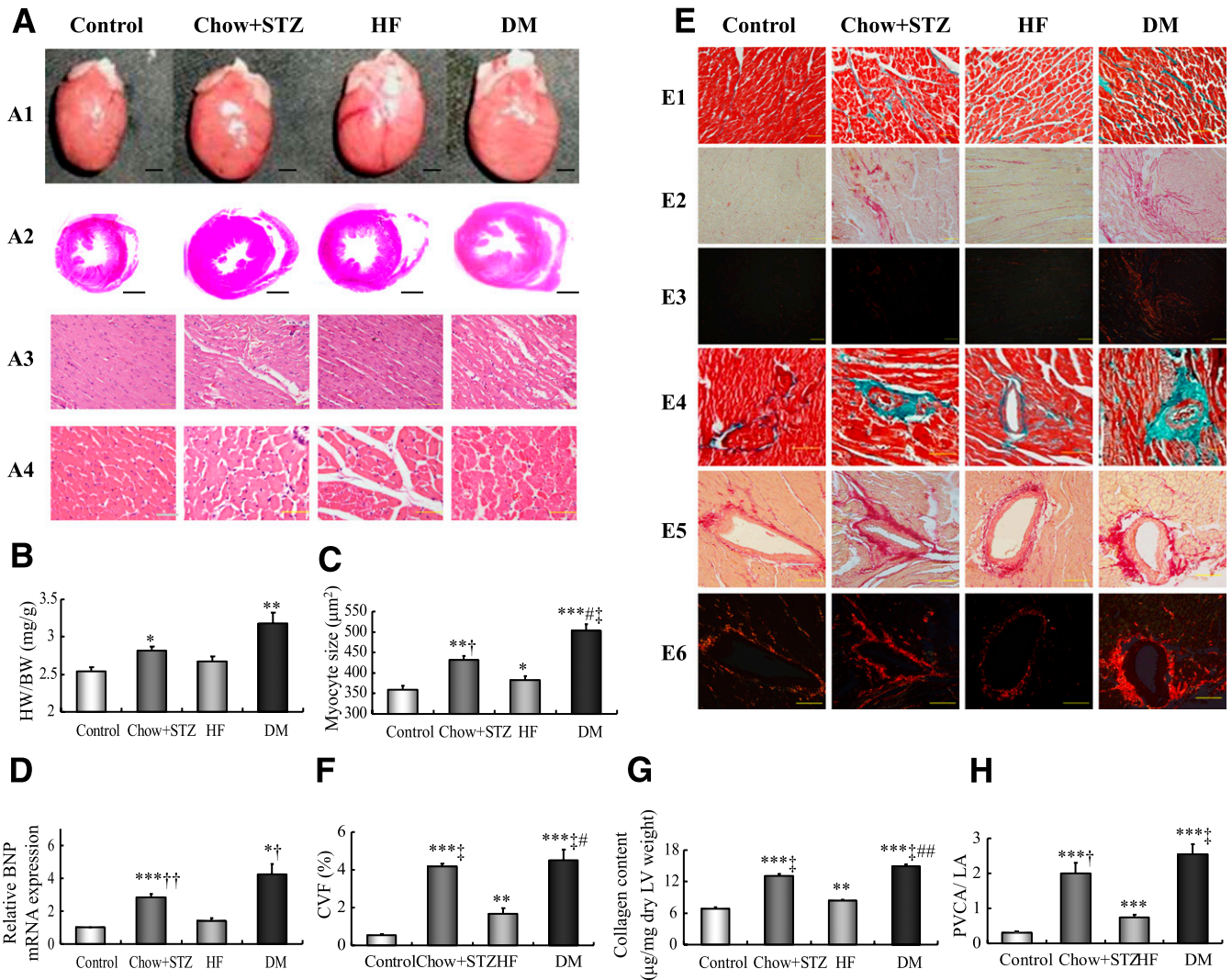


FIG. 3. Pathology features of DCM. Cardiac hypertrophy in diabetic (DM) rats. A1: Heart size (scale bar: 2 mm). **A2:** Representative cross sections of hearts at the papillary muscle level (scale bar: 2 mm). **A3:** Longitudinal sections of LV stained with hematoxylin and eosin (H&E; scale bar: 50 μm). **A4:** Transverse sections of LV stained with H&E (scale bar: 50 μm). **B:** Quantitative data of heart weight to body weight (HW-to-BW) ratio. **C:** Morphometric quantification of myocyte size. **D:** Relative mRNA expression of brain natriuretic protein (BNP). **E:** Cardiac fibrosis in diabetic rats is shown. Masson trichrome staining (collagen is green and myocardium red; scale bar: 50 μm [E1]) and Picrosirius red staining (collagen fibers stained bright red, bright-field [E2], dark-field [E3]; scale bar: 100 μm) show interstitial fibrosis. Masson trichrome staining (E4) (scale bar: 100 μm) and Picrosirius red staining (bright-field [E5], dark-field [E6]; scale bar: 100 μm) show perivascular fibrosis. **F:** Quantitative analysis of CVF. **G:** Collagen content determined by hydroxyproline assay. **H:** Quantitative analysis of PVCA/LA. Data are mean ± SEM; n = 6. *P < 0.05, **P < 0.01, ***P < 0.001 vs. control; †P < 0.05, ††P < 0.01, †††P < 0.001 vs. HF; #P < 0.05, ##P < 0.01 vs. chow + STZ. (A high-quality digital representation of this figure is available in the online issue.)

(Supplementary Fig. 1A3 and A4). Thus, the diabetic group showed insulin resistance after a 4-week HF diet.

At the end of the experiment, the diabetic group showed impaired glucose tolerance on IPGTT compared with the other three groups; blood glucose levels especially were significantly elevated at all time points compared with the control (P < 0.05) (Supplementary Fig. 1B1). The diabetic group showed the highest mean AUC on both IPGTT and IPITT (Supplementary Fig. 1B2 and B4). Similarly, the chow + STZ and HF groups showed higher mean AUC on both IPGTT and IPITT compared with the control (P < 0.05) (Supplementary Fig. 1B2 and B4).

Total cholesterol, triglyceride, FFA, and FBG concentrations. The biochemical values are given in Fig. 1. After 4 weeks of an HF diet, serum triglyceride and FFA levels were significantly higher in the HF and diabetic groups than in the control and chow + STZ groups (P < 0.05). The

ISI was markedly decreased in the HF and diabetic groups (P < 0.05). Insulin resistance appeared at week 4 in rats fed an HF diet. One week after STZ injection, FBG was remarkably elevated in the diabetic group and remained elevated until the end of the experiment. ISI consistently decreased in the diabetic group after the onset of diabetes. Simultaneously, in the diabetic group, serum total cholesterol, total triglyceride, and FFA levels were maintained at higher levels than the control (P < 0.05) during diabetes. Thus, the diabetic model induced by an HF diet and low-dose STZ was characterized by insulin resistance, moderate hyperglycemia, and hyperlipidemia, resembling the state of chemical diabetes in humans.

LV dysfunction assessed by echocardiography and catheterization. We evaluated ejection fraction, FS, E/A, and E'/A' to investigate changes in systolic and diastolic

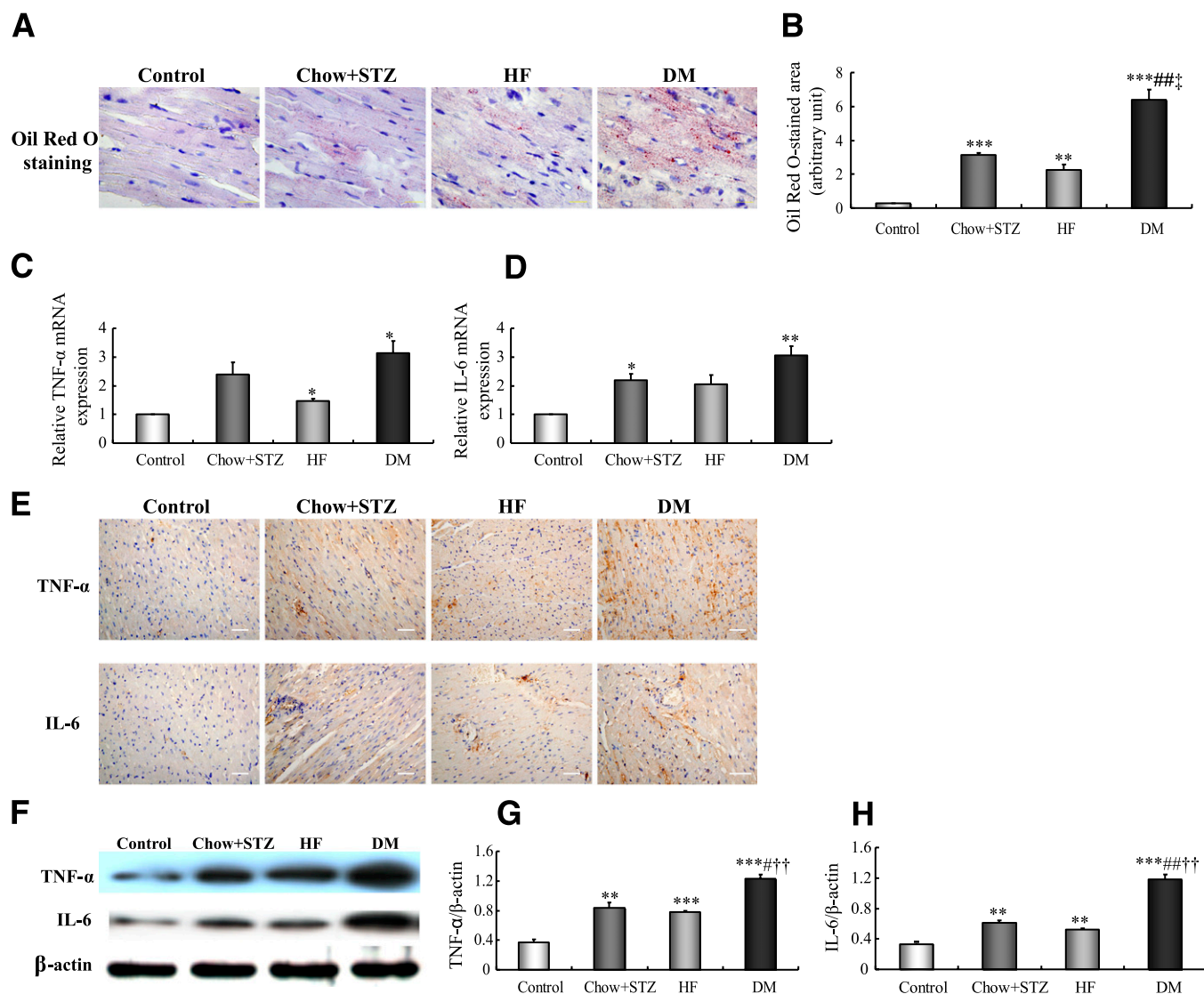


FIG. 4. Diabetic (DM) rats showed excessive myocardial lipids deposition and inflammation. **A:** Representative Oil Red O–stained myocardial sections (scale bar: 20 μ m). **B:** Semiquantification of Oil Red O staining. Data are mean \pm SEM of six independent observations in each group. **C** and **D:** Relative mRNA expression of myocardial TNF- α and IL-6. **E:** Immunohistochemical staining for myocardial TNF- α and IL-6 (brown staining considered positive staining; scale bar: 50 μ m). **F:** Representative Western blot of myocardial TNF- α and IL-6. **G** and **H:** Western blot analyses of TNF- α (**G**) and IL-6 (**H**). Data are mean \pm SEM. * P < 0.05, ** P < 0.01, *** P < 0.001 vs. control; †† P < 0.01, ‡ P < 0.001 vs. HF; # P < 0.05, ## P < 0.01 vs. chow + STZ. (A high-quality digital representation of this figure is available in the online issue.)

function. Similar to the pattern in humans, in rats, diastolic dysfunction precedes systolic dysfunction, beginning from 2 to 3 months after the induction of diabetes (26). In our study, at 6 weeks after the onset of diabetes (at week 11), the diabetic rats showed a moderate decrease in E/A and E'/A' compared with the control (P < 0.05) (Fig. 2E and F); LVEF and FS were impaired from week 17 (Fig. 2C and D). At the end of the experiment, LVEF, FS, E/A, and E'/A' were further decreased in the diabetic group, with the reduction in E/A and E'/A' more pronounced. LVEF, FS, E/A, and E'/A' were also reduced in the chow + STZ group compared with the control (P < 0.05) (Fig. 2C–F) at the end of the experiment. Left ventricular end-diastolic diameter was the highest in the diabetic group (Fig. 2B).

To further confirm the LV diastolic dysfunction, LVEDP was measured by cardiac catheterization. Diabetic rats had the highest LV pressure (Fig. 2H and I). The chow + STZ and HF groups showed higher LV pressure compared with the control (P < 0.01 ~ P < 0.001) (Fig. 2H and I). In summary,

both systolic and diastolic dysfunction developed and progressed during DCM, with predominant deterioration of diastolic function.

Pathology characteristics of diabetic rats. The heart weight to body weight ratio was 25% higher in the diabetic group than the control group (P < 0.01) (Fig. 3B), and LV myocyte size was 40 and 31% higher, respectively, than the control and HF groups (P < 0.001) (Fig. 3C). Furthermore, the relative mRNA expression of brain natriuretic protein, a marker of LV hypertrophy (27), was higher in diabetic than control and HF rats (P < 0.05) (Fig. 3D).

The diabetic group showed cardiac fibrosis, with a diffuse, small, patchy, and nonuniform pattern, as well as destroyed and disorganized collagen network structure in the interstitial (Fig. 3E1–E3) and perivascular (Fig. 3E4–E6) areas. CVF and collagen content were higher in the diabetic group than the other groups (P < 0.05 ~ P < 0.001) (Fig. 3F and G), as was PVCA/LA (P < 0.001) (Fig. 3H). These histological changes were confirmed by echocardiographic

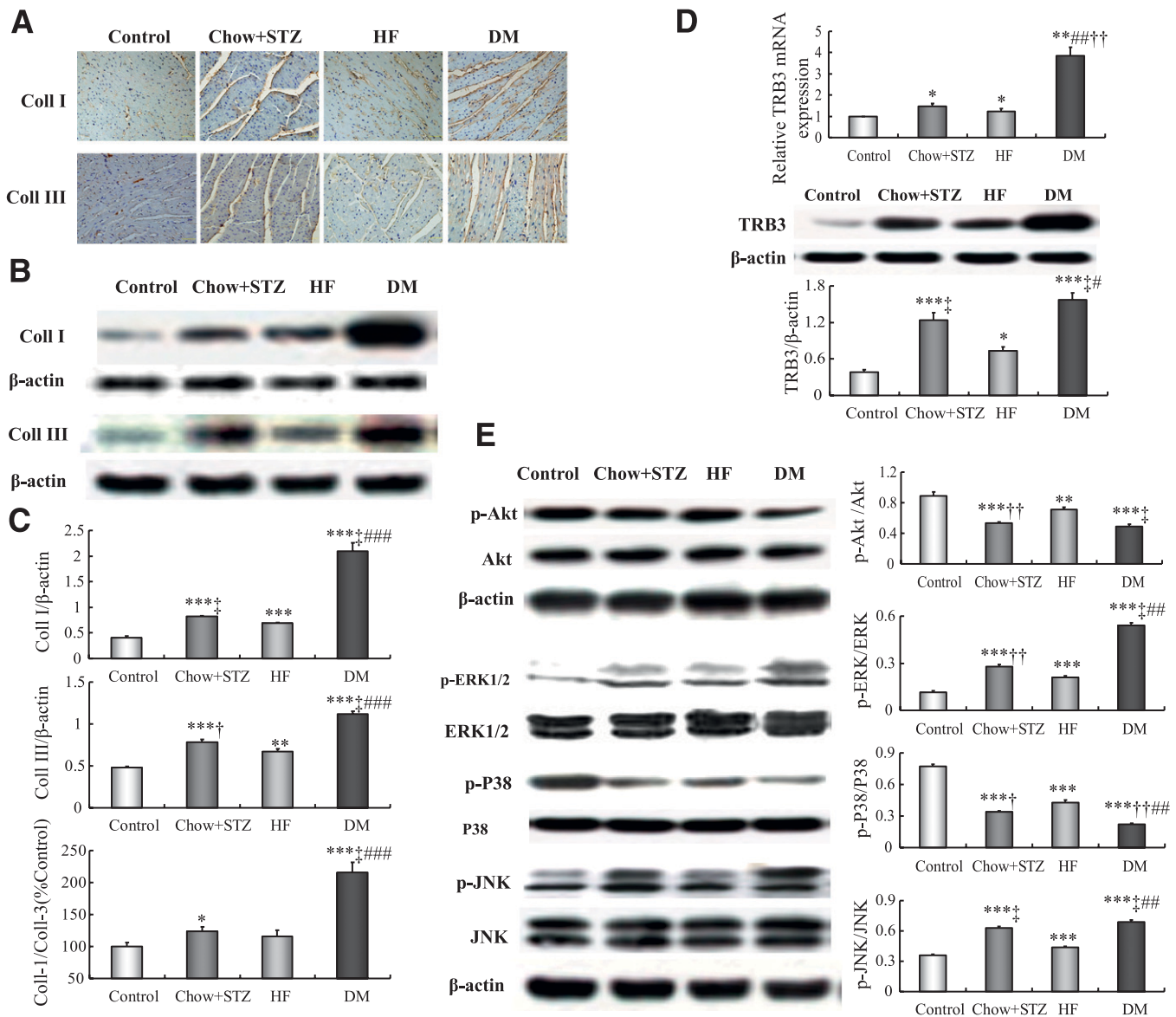


FIG. 5. Diabetes increases collagen I (coll I) and collagen III (coll III) content, suppresses Akt phosphorylation, and partly activates TRB3/MAPK pathway. *A:* Representative immunohistochemical staining of collagen I and III (brown staining considered positive staining; scale bar: 50 μm). *B:* Representative Western blot of collagen I and III content. *C:* Western blot analysis of collagen I, collagen III, and collagen I-to-III ratio. *D:* Relative mRNA expression and protein content of myocardial TRB3. *E:* Western blot analysis of p-Akt/Akt, p-ERK/ERK, p-p38/p38, and p-JNK/JNK. Data are mean ± SEM. **P* < 0.05, ***P* < 0.01, ****P* < 0.001 vs. control; †*P* < 0.05, ‡*P* < 0.01, ‡‡*P* < 0.001 vs. HF; #*P* < 0.05, ##*P* < 0.01, ###*P* < 0.001 vs. chow + STZ. DM, diabetic rats. (A high-quality digital representation of this figure is available in the online issue.)

results. The diabetic group showed increased IB% and decreased CVIB in the interventricular septum and LV posterior and lateral walls compared with the control and HF groups (*P* < 0.05) (Supplementary Table 2). Similarly, CVF, collagen content, and PVCA/LA were significantly increased in the chow + STZ and HF groups compared with the control (*P* < 0.01 ~ *P* < 0.001) (Fig. 3*F–H*).

Coincident with cardiac dysfunction and hypertrophy, myocardial lipid analysis revealed striking myocardial accumulation of triglycerides in diabetic rats (Fig. 4*A* and *B*). Diabetic rats had higher Oil Red O-staining areas than other groups (Fig. 4*B*). The mRNA expression levels of TNF-α and IL-6 were significantly higher in the diabetic group compared with the control (*P* < 0.05, *P* < 0.01) (Fig. 4*C* and *D*). The protein expression levels of TNF-α and IL-6 were significantly increased in the diabetic group compared with the

other three groups (Fig. 4*E–H*). Likewise, the protein expression of TNF-α and IL-6 content was increased in the chow + STZ and HF groups compared with the control (*P* < 0.01 ~ *P* < 0.001) (Fig. 4*F–H*).

Immunohistochemistry and Western blot analysis revealed the protein expression of collagen I and III content increased in the diabetic group (Fig. 5*A* and *B*), and the collagen I-to-III ratio significantly elevated compared with the control group (216 ± 16% vs. 100 ± 6%, respectively; *P* < 0.001) (Fig. 5*C*). Likewise, the protein expression of collagen I and III content was increased in the chow + STZ and HF groups compared with the control (*P* < 0.01 ~ *P* < 0.001) (Fig. 5*A–C*).

These results show the established type 2 DCM model, with insulin resistance, severe LV dysfunction, and myocardial remodeling.

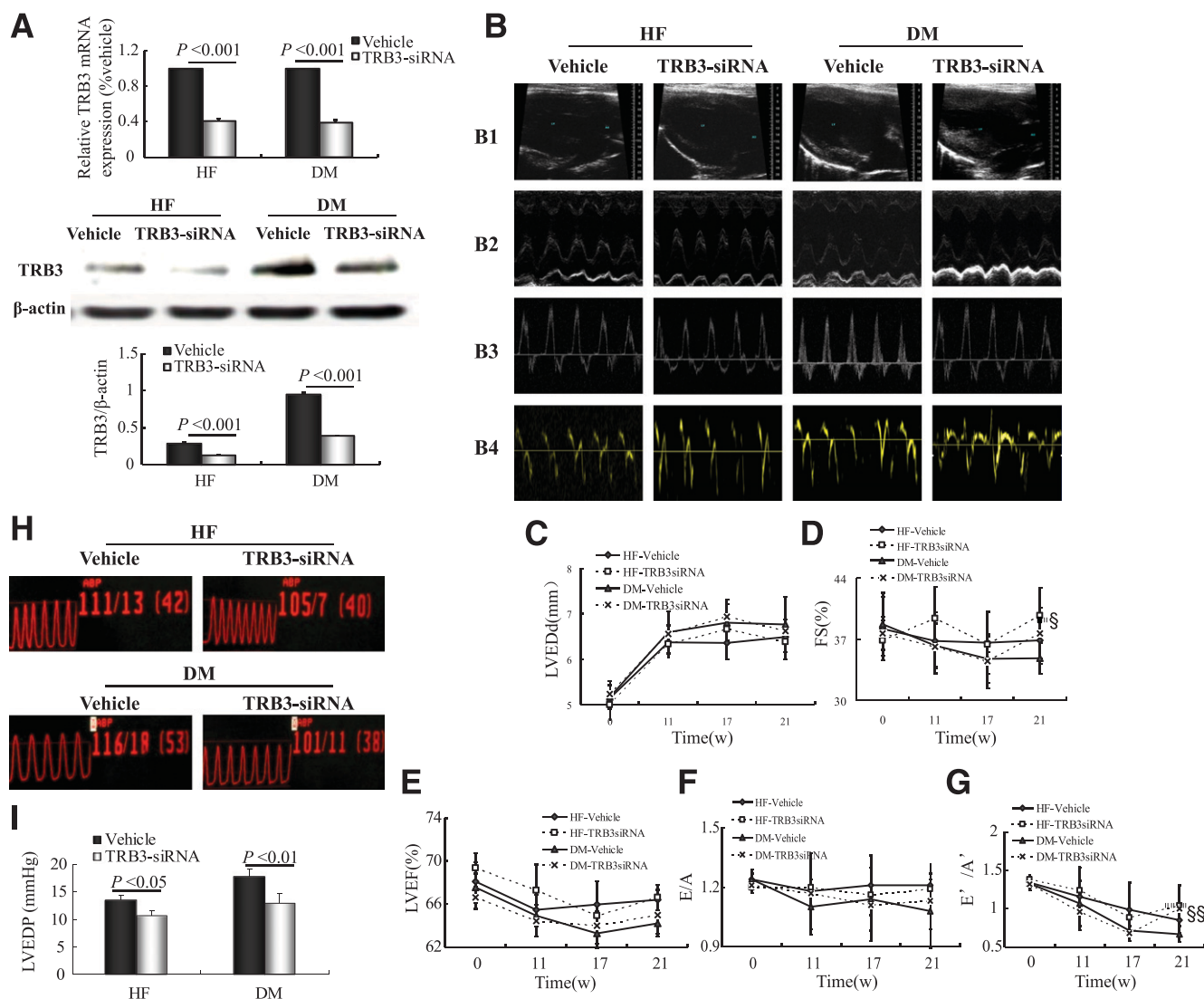


FIG. 6. *TRB3* gene therapy improves cardiac function in diabetic (DM) rats. **A:** Relative mRNA expression and protein content of myocardial *TRB3* in gene-silencing groups. **B:** Representative echocardiograms. **C–G:** Sequential evaluations of left ventricular end diastolic diameter (LVEDd) (**C**), FS (**D**), LVEF (**E**), E/A (**F**), and E'/A' (**G**). **H:** Pressure curves of cardiac catheterization. **I:** Analysis of LVEDP with *TRB3*-siRNA silencing. Data are mean \pm SEM; $n = 7$ –10 per group. $\$P < 0.05$, $\$\$P < 0.01$ vs. DM + vehicle. w, weeks. (A high-quality digital representation of this figure is available in the online issue.)

Activated TRB3/MAPK signaling pathway in DCM. Cardiac *TRB3* mRNA and protein expression was significantly increased in diabetic rats (Fig. 5D). We detected Akt expression in the myocardium. The phosphorylation of Akt was significantly lower in the diabetic group than in the control and HF groups (Fig. 5E).

Accompanied by *TRB3* overexpression, the phosphorylation of ERK1/2 and JNK was markedly increased, whereas that of p38 MAPK was decreased (Fig. 5E), which suggested that the *TRB3*/MAPK signaling pathway participates in the pathogenesis of DCM.

***TRB3* gene silencing reverses DCM**

Detection of cardiac *TRB3* expression by Western blot analysis after gene silencing. When compared with vehicle treatment, *TRB3*-siRNA treatment conferred downregulated mRNA and protein expression of cardiac *TRB3* (Fig. 6A). The mRNA and protein expression of hepatic *TRB3* was also downregulated compared with the vehicles (Supplementary Fig. 2).

***TRB3* gene silencing ameliorated metabolism.** Water intake and urine volume were decreased in the diabetic group with *TRB3*-siRNA treatment (Supplementary Table 3). The elevated serum levels of total cholesterol, triglyceride, FFA, and FBG were greatly reduced after 4-week transfection (Supplementary Fig. 3A–D).

***TRB3* gene silencing improved glucose tolerance and insulin sensitivity.** With *TRB3* gene silencing, ISI was higher in the diabetic *TRB3*-siRNA group than vehicle (-5.17 ± 0.14 vs. -5.67 ± 0.14 , respectively; $P < 0.05$) (Supplementary Fig. 3F). With *TRB3*-siRNA treatment, IPGTT and IPITT results showed a blood glucose level significantly lower for *TRB3*-siRNA-treated rats than the vehicle group ($P < 0.05$) (Supplementary Fig. 4A and B). The AUC for glucose and insulin was lower for the diabetic than the vehicle group ($P < 0.05$) (Supplementary Fig. 4C and D). The *TRB3*-siRNA HF group showed lower mean AUC on both IPGTT and IPITT than the vehicle group ($P < 0.05$) (Supplementary Fig. 4C and D).

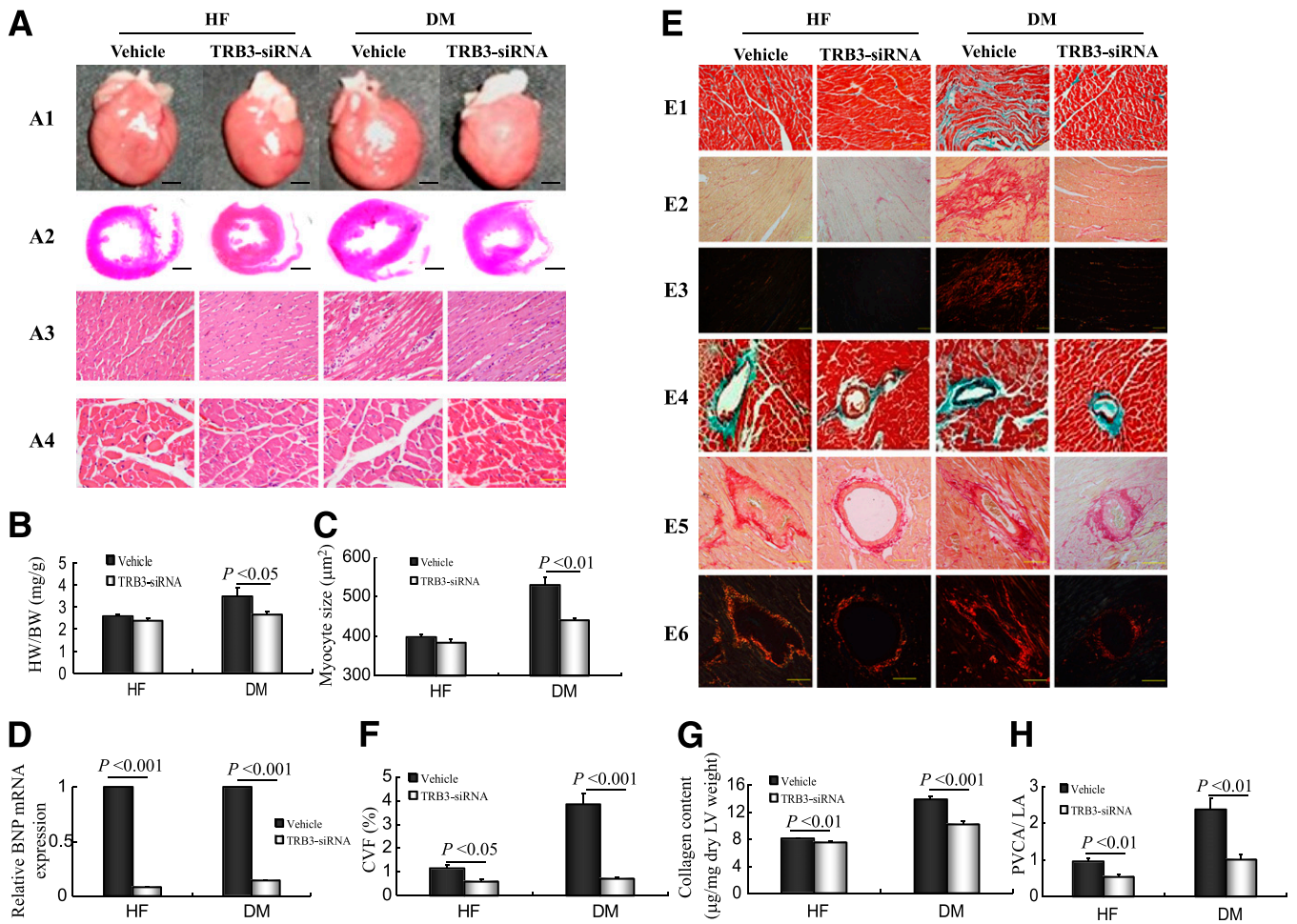


FIG. 7. *TRB3* gene therapy decreases myocardial hypertrophy and fibrosis in HF and diabetic (DM) groups. *A1*: Heart size (scale bar: 2 mm). *A2*: Representative cross sections of hearts at the papillary muscle level (scale bar: 2 mm). *A3*: Longitudinal sections of LV stained with hematoxylin and eosin (H&E) (scale bar: 50 μm). *A4*: Transverse section of LV stained with H&E (scale bar: 50 μm). *B–D*: Quantitative data for heart weight to body weight (HW-to-BW) ratio, myocyte size, and relative brain natriuretic protein (BNP) mRNA expression. *E1–6*: Representative Masson trichrome staining and Picrosirius red staining. *F–H*: Quantitative analyses of CVF, collagen content, and PVCA/LA. Data are mean \pm SEM; $n = 7–10$ per group. (A high-quality digital representation of this figure is available in the online issue.)

Recovery of cardiac function in DCM after *TRB3* silencing. During the 4-week follow-up after *TRB3*-siRNA treatment, FS and E'/A' were improved in the diabetic group compared with the vehicle group (FS, 37.66 ± 1.09 vs. 34.83 ± 0.57 , $P < 0.05$; E'/A' , 1.08 ± 0.11 vs. 0.67 ± 0.03 , $P < 0.01$) (Fig. 6D and G), which suggests that *TRB3*-siRNA treatment prevented LV dysfunction. The decreased LVEDP in the *TRB3*-siRNA diabetic group compared with the vehicle group (12.93 ± 1.77 vs. 17.77 ± 1.29 mmHg, respectively; $P < 0.01$) (Fig. 6I) reconfirmed the beneficial effect of *TRB3*-siRNA on improving LV diastolic dysfunction. Likewise, the LVEDP was reduced in the *TRB3*-siRNA HF group compared with the vehicle group ($P < 0.05$) (Fig. 6J). ***TRB3* gene silencing reverses myocardial remodeling, lipids accumulation, and cardiac inflammation in DCM.** With *TRB3*-siRNA treatment, heart weight-to-body weight ratio and myocyte size were significantly decreased in the diabetic versus the vehicle group (heart weight-to-body weight ratio: 2.67 ± 0.13 vs. 3.49 ± 0.36 mg/g, $P < 0.05$; myocyte size: 384.32 ± 8.69 vs. 440.14 ± 4.47 μm^2 , $P < 0.01$) (Fig. 7B and C). The mRNA expression of brain natriuretic protein was lower in both the HF and diabetic groups than in the vehicle control ($P < 0.001$)

(Fig. 7D). CVF and PVCA/LA were reduced ($P < 0.001$, $P < 0.01$) (Fig. 7F and H). In addition, collagen content was lower in the diabetic group than the vehicle group (10.17 ± 0.41 vs. 13.84 ± 0.48 $\mu\text{g}/\text{mg}$ LV weight, respectively; $P < 0.001$) (Fig. 7G). Likewise, CVF and PVCA/LA were decreased in the *TRB3*-siRNA HF group ($P < 0.05$, $P < 0.01$) (Fig. 7F and H). In keeping with these observations, the decreased IB% and increased CVIB acquired from the IBS of the LV reconfirmed the improved pathological manifestations ($P < 0.05 \sim P < 0.001$) (Supplementary Table 4).

The aberrant lipids accumulation within cardiomyocytes in diabetic rats was markedly reduced after *TRB3* silencing ($P < 0.001$) (Fig. 8A and B). Immunohistochemical staining and Western blot revealed a significant decrease of TNF- α and IL-6 content in the *TRB3*-siRNA diabetic group compared with those of the vehicle ($P < 0.001$) (Fig. 8E–H). Similarly, lipids accumulation and cardiac inflammation were reduced in the *TRB3*-siRNA HF group ($P < 0.01$, $P < 0.001$) (Fig. 8B and E–H).

***TRB3* gene silencing reduced the collagen I-to-III ratio and regulated Akt and MAPK pathway.** With *TRB3*-siRNA treatment, collagen I and the collagen I-to-III ratio

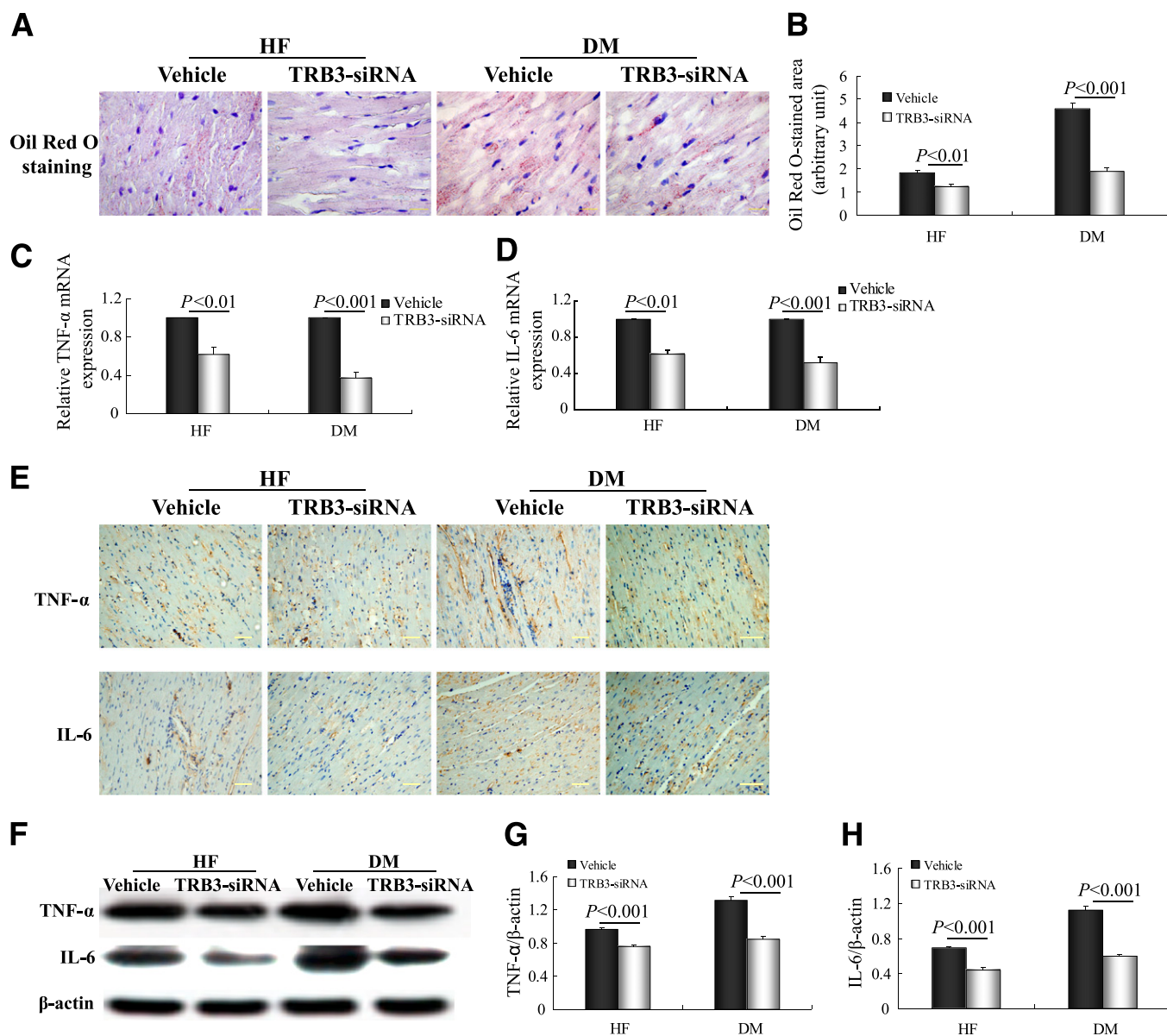


FIG. 8. *TRB3* gene silencing decreases aberrant lipid accumulation and cardiac inflammation. **A:** Representative Oil Red O-stained myocardial sections (scale bar: 20 μ m). **B:** Semi-quantification of Oil Red O staining. Data are mean \pm SEM of six independent observations in each group. **C and D:** Relative mRNA expression of myocardial TNF- α and IL-6. **E:** Immunohistochemical staining for myocardial TNF- α and IL-6 (brown staining considered positive staining; scale bar: 50 μ m). **F:** Representative Western blot of myocardial TNF- α and IL-6. **G and H:** Western blot analyses of TNF- α (**G**) and IL-6 (**H**). Data are mean \pm SEM. DM, diabetic rats. (A high-quality digital representation of this figure is available in the online issue.)

were lower in the diabetic than vehicle group ($P < 0.001$) (Fig. 9B and C). The decrease in collagen III content was not as great as that of collagen I ($P < 0.01$) (Fig. 9B and C).

The inhibited phosphorylation of p-Akt in the diabetic group was restored after *TRB3* silencing (Fig. 9D).

With *TRB3* silencing, the phosphorylation of ERK1/2 and JNK was abolished by 53 and 46%, respectively, in the diabetic group (Fig. 9D); however, the phosphorylation of p38 MAPK was enhanced compared with the vehicle group (Fig. 9D). Thus, *TRB3* gene silencing appeared to have differential effects on ERK1/2, JNK, and p38 MAPK: inhibiting ERK1/2 and JNK activation (with a more pronounced effect on ERK1/2) but activating p38 MAPK.

DISCUSSION

TRB3 is associated with insulin resistance, an important trigger in the development of DCM. We found *TRB3* was

involved in the pathogenesis of DCM. *TRB3* gene silencing alleviated DCM mainly by modulating MAPK and Akt pathways in type 2 diabetes. Thus, *TRB3* has a pivotal role in DCM and could be an attractive drug target for treating type 2 diabetes.

***TRB3*, a critical mediator for insulin resistance, is implicated in DCM.** The insulin-Akt signaling pathway regulates mitogenic effects in virtually all metabolic tissues, and proteins that inhibit Akt activity are considered potential inducers of insulin resistance (28). An example of such a protein is the catalytically inactive pseudokinase *TRB3* (7). *TRB3* is overexpressed in murine models of insulin resistance (7,8). In the current study, diabetic rats showed severe insulin resistance and increased *TRB3* level. Akt activation was inhibited. These findings are in accordance with previous studies (7,8,28), which indicates insulin resistance exists in our type 2 diabetic rat model at the molecular level.

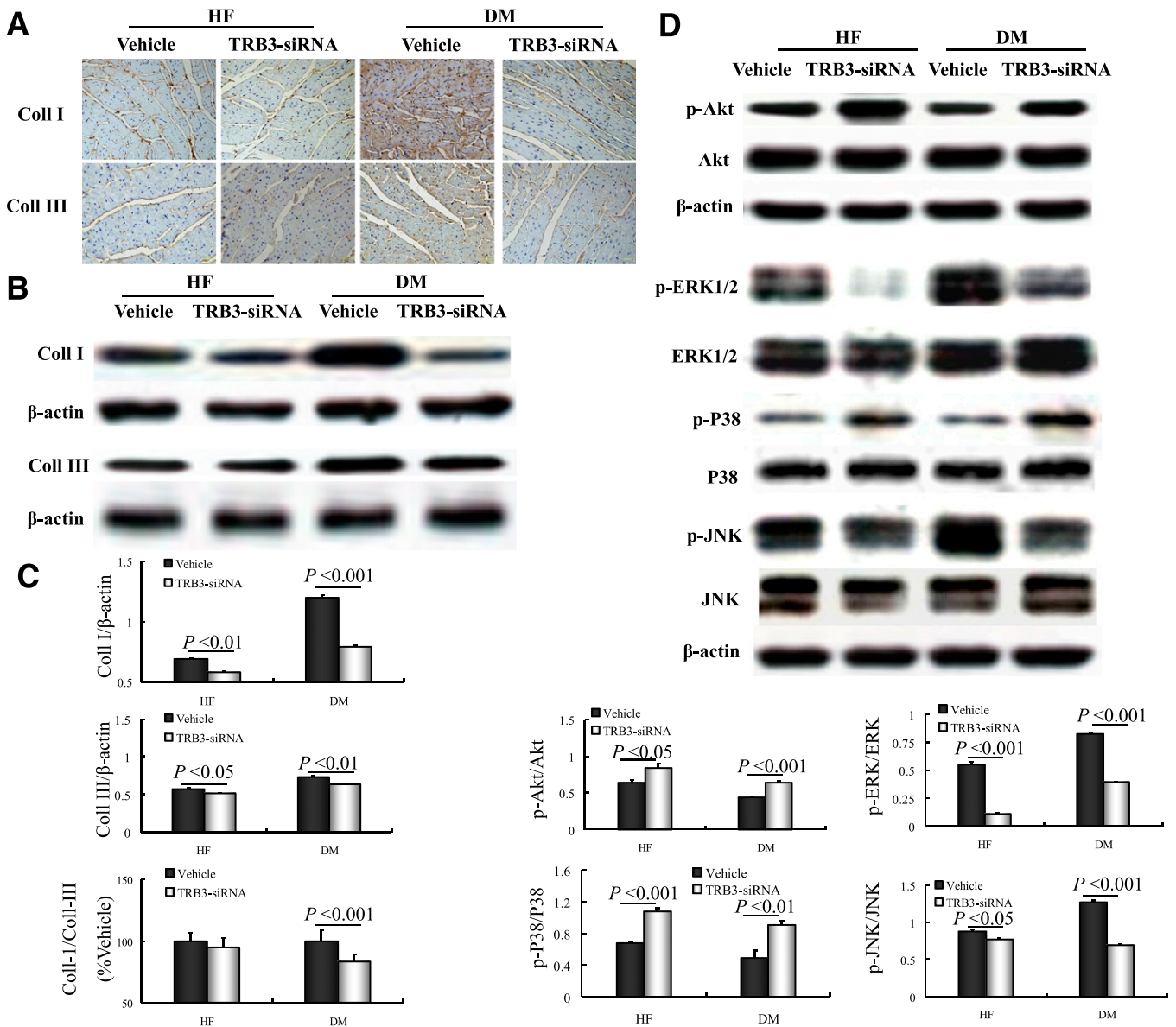


FIG. 9. *TRB3* gene silencing decreases collagen expression, restores the phosphorylation of p-Akt, and partly reverses MAPK activation. **A:** Representative immunohistochemical staining showing collagen I and III (scale bar: 50 μ m). **B:** Representative Western blot of collagen I and III. **C:** Western blot analyses of collagen I and III content and collagen I-to-III ratio. **D:** Western blot analysis of p-Akt/Akt, p-ERK/ERK, p-p38/p38MAPK, and p-JNK/JNK. Data are mean \pm SEM. DM, diabetic rats. (A high-quality digital representation of this figure is available in the online issue.)

In an insulin-resistant state, the phosphatidylinositol 3-kinase/Akt pathway appears to be selectively blunted, compared with the fully activated MAPK pathway (29). This situation is known as pathway-selective insulin resistance (12). Kiss-Toth et al. (11) reported that TRB3 might be an important modulating protein of MAPK. We found TRB3 markedly upregulated in rats with diabetes, which was paralleled by increased ERK1/2 and JNK expression. Diabetic rats showed prominent collagen accumulation in interstitial and perivascular areas on Masson trichrome and Picrosirius red staining. Increased cardiac fibrosis, which can increase LV stiffness, is a common hallmark of DCM (30). Therefore, our diabetic rats showed severe DCM, which was further confirmed by elevated LVEDP. Previous studies have shown that activated MAPK plays an essential role in collagen synthesis and cardiac fibrosis (15,31). Therefore, activation of TRB3 may contribute to the development and progression of DCM, possibly mediated by the MAPK pathway.

Together, these data suggest a pivotal role for TRB3 in selective insulin resistance by modulating Akt and MAPK pathways and implicated in the development of DCM.

Effect of *TRB3* silencing on DCM mediated by MAPK and Akt pathways. In light of the pivotal role of TRB3 in the development of DCM, we wondered whether down-regulation of TRB3 could reverse the progression of DCM. According to our previous study (14), we used TRB3-siRNA in vivo in rats. TRB3-siRNA treatment produced no notable adverse effects and no deaths in rats. TRB3 mRNA levels were significantly decreased, and the protein expression was reduced by ~60% with TRB3-siRNA treatment in diabetic rats. Thus, global silencing of *TRB3* was feasible and effective.

With *TRB3* silencing, the impaired glucose tolerance and decreased insulin sensitivity were improved, and the inhibited activation of Akt was restored. So *TRB3* silencing could improve insulin resistance and lower blood

glucose, which was attributed to increased phosphorylation of Akt (32).

In addition to improving metabolic disturbance, *TRB3* silencing reduced the aberrant interstitial and perivascular collagen accumulation, as well as total collagen content. Echocardiography and catheterization results revealed that the LV diastolic dysfunction was improved, which was attributed to decreased cardiac fibrosis and reduced collagen I-to-collagen III ratio (33). Thus, *TRB3* silencing attenuated DCM.

As discussed above, the MAPK pathway likely mediated *TRB3*-related cardiac fibrosis. Intriguingly, we found a generalized decrease in phosphorylation of JNK and especially ERK1/2 in with *TRB3* silencing. Combined with previous studies (12,14,34), the improvements in cardiac fibrosis were primarily attributed to the decreased activation of ERK1/2. So *TRB3* is an effective target to ameliorate DCM mainly through the ERK/MAPK pathway.

With silencing of *TRB3*, enhanced phosphorylation of ERK/MAPK was suppressed, whereas the impaired Akt activity was upregulated. These alterations resulted in overall improvement of selective insulin resistance. In accordance with these changes at the molecular level, *TRB3* silencing attenuated the cardiac fibrosis and metabolic disturbance in type 2 diabetic rats.

Furthermore, lipids accumulation (35) and inflammation (36) in the cardiac tissue play a pivotal role in the pathophysiology of DCM. In the current study, we also referred to these aspects. *TRB3* silencing reduced the aberrant lipids deposition and cardiac inflammation. However, the underlying mechanisms remain unclear. Further studies have to reveal the impact of *TRB3* silencing on these effects.

Conclusions. *TRB3*, as a critical regulator for selective insulin resistance, was implicated in DCM. The cardioprotective effects with *TRB3* silencing suggest a potential role for *TRB3* inhibitors in treating DCM in type 2 diabetes.

ACKNOWLEDGMENTS

This work was supported by research grants from Key Technologies R & D Program of Shandong Province (2006GG2202020 and 2010G0020262), the Natural Science Foundation of Shandong Province (Y2005C11, ZR2009CM022, ZR2009CM025, and BS2009YY026), the National Natural Science Foundation of China (30670874, 30871038, 30971215, 81070192, and 81070141), and the National Basic Research Program of China (973 Program, grant 2009CB521904).

No potential conflicts of interest relevant to this article were reported.

Y.T. and G.-I.X. researched data and wrote the manuscript. Z.-h.W. researched data and contributed to discussion. X.-I.B., W.-y.D., J.W., and G.-h.J. researched data. P.-I.B., M.Z., and W.Z. wrote, reviewed, and edited the manuscript. Y.Z. reviewed and edited the manuscript.

REFERENCES

- Poornima IG, Parikh P, Shannon RP. Diabetic cardiomyopathy: the search for a unifying hypothesis. *Circ Res* 2006;98:596-605
- Young ME, Guthrie PH, Razeghi P, et al. Impaired long-chain fatty acid oxidation and contractile dysfunction in the obese Zucker rat heart. *Diabetes* 2002;51:2587-2595
- Witteles RM, Fowler MB. Insulin-resistant cardiomyopathy clinical evidence, mechanisms, and treatment options. *J Am Coll Cardiol* 2008;51:93-102
- Yang ZH, Peng XD. Insulin resistance and heart injury in rats with insulin resistance or type 2 diabetes mellitus. *Acta Cardiol* 2010;65:329-335
- Iacobellis G, Ribaldo MC, Zappaterreno A, et al. Relationship of insulin sensitivity and left ventricular mass in uncomplicated obesity. *Obes Res* 2003;11:518-524
- Dinh W, Lankisch M, Nickl W, et al. Insulin resistance and glycemic abnormalities are associated with deterioration of left ventricular diastolic function: a cross-sectional study. *Cardiovasc Diabetol* 2010;9:63
- Du K, Herzig S, Kulkarni RN, Montminy M. *TRB3*: a tribbles homolog that inhibits Akt/PKB activation by insulin in liver. *Science* 2003;300:1574-1577
- Koo S-H, Satoh H, Herzig S, et al. PGC-1 promotes insulin resistance in liver through PPAR- α -dependent induction of *TRB3*. *Nat Med* 2004;10:530-534
- Prudente S, Hribal ML, Flex E, et al. The functional Q84R polymorphism of mammalian Tribbles homolog *TRB3* is associated with insulin resistance and related cardiovascular risk in Caucasians from Italy. *Diabetes* 2005;54:2807-2811
- Gong HP, Wang ZH, Jiang H, et al. *TRB3* functional Q84R polymorphism is a risk factor for metabolic syndrome and carotid atherosclerosis. *Diabetes Care* 2009;32:1311-1313
- Kiss-Toth E, Bagstaff SM, Sung HY, et al. Human tribbles, a protein family controlling mitogen-activated protein kinase cascades. *J Biol Chem* 2004;279:42703-42708
- Jiang ZY, Lin YW, Clemont A, et al. Characterization of selective resistance to insulin signaling in the vasculature of obese Zucker (fa/fa) rats. *J Clin Invest* 1999;104:447-457
- Papakrivopoulou J, Lindahl GE, Bishop JE, Laurent GJ. Differential roles of extracellular signal-regulated kinase 1/2 and p38MAPK in mechanical load-induced procollagen alpha1(I) gene expression in cardiac fibroblasts. *Cardiovasc Res* 2004;61:736-744
- Tang M, Zhong M, Shang Y, et al. Differential regulation of collagen types I and III expression in cardiac fibroblasts by AGEs through *TRB3*/MAPK signaling pathway. *Cell Mol Life Sci* 2008;65:2924-2932
- Satomi-Kobayashi S, Ueyama T, Mueller S, et al. Deficiency of nectin-2 leads to cardiac fibrosis and dysfunction under chronic pressure overload. *Hypertension* 2009;54:825-831
- Sahn DJ, DeMaria A, Kisslo J, Weyman A. Recommendations regarding quantitation in M-mode echocardiography: results of a survey of echocardiographic measurements. *Circulation* 1978;58:1072-1083
- Di Paola R, Di Guardo G, Lo Giudice P, Caruso V, Magnano C, Mangiameli S. Preclinical thalassemic cardiopathy: a study by acoustic densitometry. *Ital Heart J* 2003;4:413-418
- Kanda T, Hayashi K, Wakino S, et al. Role of Rho-kinase and p27 in angiotensin II-induced vascular injury. *Hypertension* 2005;45:724-729
- Sun M, Dawood F, Wen WH, et al. Excessive tumor necrosis factor activation after infarction contributes to susceptibility of myocardial rupture and left ventricular dysfunction. *Circulation* 2004;110:3221-3228
- Peng H, Carretero OA, Raji L, Yang F, Kapke A, Rhaleb NE. Antifibrotic effects of N-acetyl-seryl-aspartyl-Lysyl-proline on the heart and kidney in aldosterone-salt hypertensive rats. *Hypertension* 2001;37:794-800
- Chiariello M, Ambrosio G, Cappelli-Bigazzi M, Perrone-Filardi P, Brigante F, Sifola C. A biochemical method for the quantitation of myocardial scarring after experimental coronary artery occlusion. *J Mol Cell Cardiol* 1986;18:283-290
- Sun M, Chen M, Dawood F, et al. Tumor necrosis factor- α mediates cardiac remodeling and ventricular dysfunction after pressure overload state. *Circulation* 2007;115:1398-1407
- Bi XP, Tan HW, Xing SS, et al. Overexpression of *TRB3* gene in adipose tissue of rats with high fructose-induced metabolic syndrome. *Endocr J* 2008;55:747-752
- Højlund K, Mogensen M, Sahlin K, Beck-Nielsen H. Mitochondrial dysfunction in type 2 diabetes and obesity. *Endocrinol Metab Clin North Am* 2008;37:713-731, x
- Hanley AJ, Karter AJ, Festa A, et al.; Insulin Resistance Atherosclerosis Study. Factor analysis of metabolic syndrome using directly measured insulin sensitivity: The Insulin Resistance Atherosclerosis Study. *Diabetes* 2002;51:2642-2647
- Yoon YS, Uchida S, Masuo O, et al. Progressive attenuation of myocardial vascular endothelial growth factor expression is a seminal event in diabetic cardiomyopathy: restoration of microvascular homeostasis and recovery of cardiac function in diabetic cardiomyopathy after replenishment of local vascular endothelial growth factor. *Circulation* 2005;111:2073-2085
- Wang J, Xu N, Feng X, et al. Targeted disruption of *Smad4* in cardiomyocytes results in cardiac hypertrophy and heart failure. *Circ Res* 2005;97:821-828
- Taniguchi CM, Emanuelli B, Kahn CR. Critical nodes in signalling pathways: insights into insulin action. *Nat Rev Mol Cell Biol* 2006;7:85-96

29. Kim JA, Montagnani M, Koh KK, Quon MJ. Reciprocal relationships between insulin resistance and endothelial dysfunction: molecular and pathophysiological mechanisms. *Circulation* 2006;113:1888–1904
30. Asbun J, Villarreal FJ. The pathogenesis of myocardial fibrosis in the setting of diabetic cardiomyopathy. *J Am Coll Cardiol* 2006;47:693–700
31. Ghosh AK, Bradham WS, Gleaves LA, et al. Genetic deficiency of plasminogen activator inhibitor-1 promotes cardiac fibrosis in aged mice: involvement of constitutive transforming growth factor- β signaling and endothelial-to-mesenchymal transition. *Circulation* 2010;122:1200–1209
32. Cho H, Mu J, Kim JK, et al. Insulin resistance and a diabetes mellitus-like syndrome in mice lacking the protein kinase Akt2 (PKB β). *Science* 2001;292:1728–1731
33. Pauschinger M, Knopf D, Petschauer S, et al. Dilated cardiomyopathy is associated with significant changes in collagen type I/III ratio. *Circulation* 1999;99:2750–2756
34. Olson ER, Shamhart PE, Naugle JE, Meszaros JG. Angiotensin II-induced extracellular signal-regulated kinase 1/2 activation is mediated by protein kinase Cdelta and intracellular calcium in adult rat cardiac fibroblasts. *Hypertension* 2008;51:704–711
35. Finck BN, Han X, Courtois M, et al. A critical role for PPARalpha-mediated lipotoxicity in the pathogenesis of diabetic cardiomyopathy: modulation by dietary fat content. *Proc Natl Acad Sci USA* 2003;100:1226–1231
36. Wellen KE, Hotamisligil GS. Inflammation, stress, and diabetes. *J Clin Invest* 2005;115:1111–1119